

## Role of Nanoparticle Valency in the Nondestructive Magnetic-Relaxation-Mediated Detection and Magnetic Isolation of Cells in Complex Media

Charalambos Kaittanis,<sup>†,‡</sup> Santimukul Santra,<sup>†</sup> and J. Manuel Perez<sup>\*,†,‡,§</sup>

Nanoscience Technology Center, Burnett School of Biomedical Sciences - College of Medicine,  
and Department of Chemistry, University of Central Florida, 12424 Research Parkway,  
Suite 400, Orlando, Florida 32826

Received May 28, 2009; E-mail: jmperez@mail.ucf.edu

**Abstract:** Nanoparticle-based diagnostics typically involve the conjugation of targeting ligands to the nanoparticle to create a sensitive and specific nanosensor that can bind and detect the presence of a target, such as a bacterium, cancer cell, protein, or DNA sequence. Studies that address the effect of multivalency on the binding and detection pattern of these nanosensors, particularly on magnetic relaxation nanosensors that sense the presence of a target in a dose-dependent manner by changes in the water relaxation times ( $\Delta T_2$ ), are scarce. Herein, we study the effect of multivalency on the detection profile of cancer cells and bacteria in complex media, such as blood and milk. In these studies, we conjugated folic acid at two different densities (low-folate and high-folate) on polyacrylic-acid-coated iron oxide nanoparticles and studied the interaction of these magnetic nanosensors with cancer cells expressing the folate receptor. Results showed that the multivalent high-folate magnetic relaxation nanosensor performed better than its low folate counterpart, achieving single cancer cell detection in blood samples within 15 min. Similar results were also observed when a high molecular weight anti-folate antibody (MW 150 kDa) was used instead of the low molecular weight folic acid ligand (MW 441.4 kDa), although better results in terms of sensitivity, dynamic range, and speed of detection were obtained when the folate ligand was used. Studies using bacteria in milk suspensions corroborated the results observed with cancer cells. Taken together, these studies demonstrate that nanoparticle multivalency plays a key role in the interaction of the nanoparticle with the cellular target and modulate the behavior and sensitivity of the assay. Furthermore, as detection with magnetic relaxation nanosensors is a nondestructive technique, magnetic isolation and further characterization of the cancer cells is possible.

### Introduction

The enhanced binding of multiple ligands to a particular cellular target is a common approach in nature to fine-tune molecular and cellular recognitions with increased specificity.<sup>1–11</sup> This kind of multivalent binding strategy can offer unique

advantages for developing selective and highly sensitive nanoparticle-based diagnostics and effective therapeutics. Nanoparticles with multiple targeting ligands offer the advantage of a surface-mediated multivalent affinity, resulting from multiple interactions between the high local concentration of binding ligands on the nanoparticle's surface and epitopes on the corresponding target. In particular, the conjugation of multiple targeting ligands to iron oxide nanoparticles (IONP) has allowed the creation of multivalent magnetic relaxation nanosensors (MRnS) for the detection of molecular targets and events, such as DNA, RNA, proteins, enzymatic activity, small molecule, viruses, enzymatic and metabolic activity.<sup>12–16</sup> Detection is achieved by changes in the solution's water relaxation times ( $\Delta T_2$ ), as these nanosensors self-assemble upon interaction with the specific target. However, all these cases shared a common target characteristic: the target was smaller than or roughly the

<sup>†</sup> Nanoscience Technology Center.

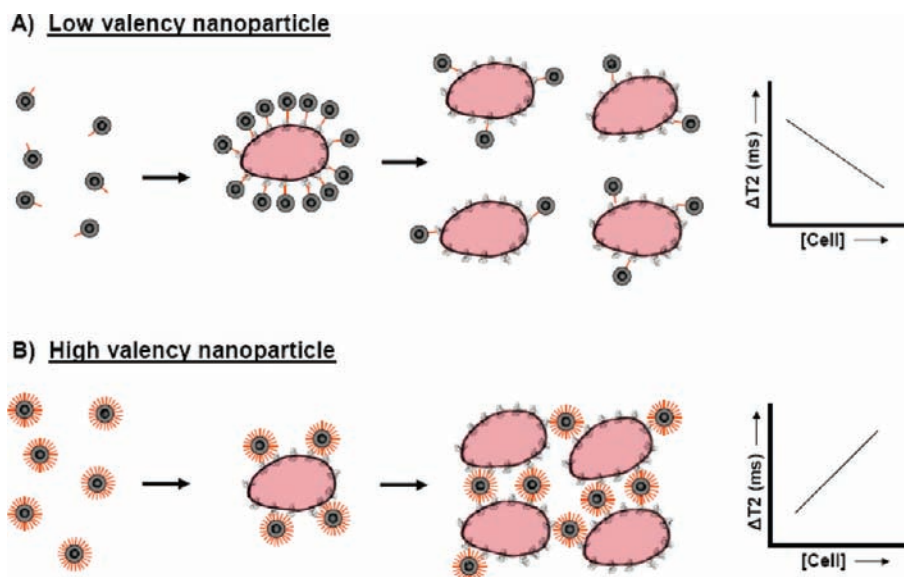
<sup>‡</sup> Burnett School of Biomedical Sciences - College of Medicine.

<sup>§</sup> Department of Chemistry.

- (1) Badjic, J. D.; Nelson, A.; Cantrill, S. J.; Turnbull, W. B.; Stoddart, J. F. *Acc. Chem. Res.* **2005**, *38*, 723–732.
- (2) Collins, B. E.; Paulson, J. C. *Curr. Opin. Chem. Biol.* **2004**, *8*, 617–625.
- (3) Greenspan, N. S. *Adv. Cancer Res.* **2001**, *80*, 147–187.
- (4) Jo, E. K. *Curr. Opin. Infect. Dis.* **2008**, *21*, 279–286.
- (5) Kiessling, L. L.; Gestwicki, J. E.; Strong, L. E. *Angew. Chem., Int. Ed.* **2006**, *45*, 2348–2368.
- (6) Larsen, M.; Artym, V. V.; Green, J. A.; Yamada, K. M. *Curr. Opin. Cell. Biol.* **2006**, *18*, 463–471.
- (7) Mathai, M.; Seok-Ki, C.; Whitesides, G. M. *Angew. Chem., Int. Ed.* **2006**, *45*, 2754–2794.
- (8) Mulder, A.; Huskens, J.; Reinhoudt, D. N. *Org. Biomol. Chem.* **2004**, *2*, 3409–3424.
- (9) Ramsay, A. G.; Marshall, J. F.; Hart, I. R. *Cancer Metastasis Rev.* **2007**, *26*, 567–578.
- (10) Schwartz, M. A.; DeSimone, D. W. *Curr. Opin. Cell Biol.* **2008**, *20*, 551–556.
- (11) Zutter, M. M. *Adv. Exp. Med. Biol.* **2007**, *608*, 87–100.

- (12) Grimm, J.; Perez, J. M.; Josephson, L.; Weissleder, R. *Cancer Res.* **2004**, *64*, 639–643.
- (13) Kaittanis, C.; Nath, S.; Perez, J. M. *PLoS ONE* **2008**, *3*, e3253.
- (14) Perez, J. M.; Grimm, J.; Josephson, L.; Weissleder, R. *Neoplasia* **2008**, *10*, 1066–1072.
- (15) Perez, J. M.; Josephson, L.; O'Loughlin, T.; Hogemann, D.; Weissleder, R. *Nat. Biotechnol.* **2002**, *20*, 816–820.
- (16) Perez, J. M.; Simeone, F. J.; Saeki, Y.; Josephson, L.; Weissleder, R. *J. Am. Chem. Soc.* **2003**, *125*, 10192–10193.

**Scheme 1.** Iron Oxide Nanoparticles' Valency Facilitates Distinct Magnetic Relaxation Sensing Trends, Which Are Modulated by the Nanoparticle–Target Interactions<sup>a</sup>



<sup>a</sup> (A) At low target concentrations, nanoparticles with low valency readily assemble on the target and cause large shifts in the  $\Delta T_2$ , whereas (B) fewer nanoparticles with high valency interact per target resulting in lower  $\Delta T_2$ . At high target concentrations, the nanoparticles with (A) low valency switch to a dispersed-like state with a concomitant  $\Delta T_2$  reduction, but (B) the ones with high valency bind and cluster between multiple targets, facilitating prominent  $\Delta T_2$  changes.

same size (in the case of a virus) as the nanosensor. Recently, the detection of a bacterium, a much larger target compared to the nanosensor, was reported.<sup>17</sup> In that report, it was found that the use of a multivalent entity (bacterium) as a biological target compensated for the size difference between the nanoprobe and the target, promoting nanoparticle assembly on the bacterial surface with concomitant target-concentration-dependent changes in  $\Delta T_2$ . It was speculated that these differences may have been attributed to the ratio of nanoparticles interacting per target, hinting that at low bacterial concentrations more nanoparticles self-assembled on the surface of the bacterium (hence higher  $\Delta T_2$ ), whereas at high bacterial concentrations fewer nanoparticles interacted per target to result in lower  $\Delta T_2$ .

Therefore, we hypothesized whether the nanoparticles' valency may affect the MRnS detection limit, allowing the engineering of ultrasensitive probes to accommodate a particular cellular concentration range. We reasoned that nanoparticles with low amounts of ligand conjugated on their surface (low valency) would assemble on the cell's surface, resulting in prominent shifts in the  $\Delta T_2$  (Scheme 1A). As the cell concentration increases, the low valency nanoparticles would switch to a quasi-dispersed state, due to their limited interaction with target moieties on discrete cells, thus causing smaller changes in the  $\Delta T_2$  at high cell concentrations (Scheme 1A). This mechanism would be in line with the reported MRnS-mediated detection of bacteria (*Mycobacterium avium* spp *paratuberculosis* - MAP) using magnetic nanoparticles conjugated with anti-MAP polyclonal antibodies, where prominent  $\Delta T_2$  was observed at low MAP amounts and low  $\Delta T_2$  was recorded at high MAP concentrations.<sup>17</sup> In contrast, we reasoned that high valency nanoparticles should not cluster in the presence of cells at low concentrations. Instead, the multiple ligands present on the high valency nanoparticle can interact with multiple receptors on the cell surface (Scheme 1B). Therefore, the interaction between

high valency nanoparticles and cells at low concentration would result in a less pronounced  $\Delta T_2$ , because a fewer number of nanoparticles may simultaneously interact with multiple receptors in a given cell. Alternatively, as the cell concentration increases, the probability of high valency nanoparticle binding to surface receptors in multiple cells increases. This should facilitate the binding of multiple ligands on the same nanoparticle with multiple receptors on different cells, causing extensive clustering of the nanoparticles and an increase in  $\Delta T_2$  as the number of cells increases. (Scheme 1B).

Hence, the lack of a comprehensive study addressing how multivalency affects the nanoparticles' cell surface assembly (e.g., bacterium or cell) and the corresponding MRnS response prompted us to utilize MRnS with engineered valency toward the detection of cancer cells in blood samples. We selected cancer cells as a model target, because it has been recently reported that viable tumor-derived epithelial cells found in circulation (circulating tumor cells) are a novel class of cancer biomarkers, participating in the initiation of the process of metastasis.<sup>18–20</sup> Current molecular diagnostic techniques cannot detect low concentrations of cells in complex media (i.e., blood),<sup>20</sup> because of the matrix's optical properties and complexity. Furthermore, commonly used cytological and immunocytochemical techniques require the cell's isolation, purification, fixation and quantification using fluorescent probes and microscopic examination, which prevent propagation of the cells

(17) Kaittanis, C.; Naser, S. A.; Perez, J. M. *Nano Lett.* **2007**, 7, 380–383.

(18) Cristofanilli, M.; Mendelsohn, J. *Proc. Natl. Acad. Sci. U.S.A.* **2006**, 103, 17073–17074.

(19) Nagrath, S.; Sequist, L. V.; Maheswaran, S.; Bell, D. W.; Irimia, D.; Ulkus, L.; Smith, M. R.; Kwak, E. L.; Digumarthy, S.; Muzikansky, A.; Ryan, P.; Balis, U. J.; Tompkins, R. G.; Haber, D. A.; Toner, M. *Nature* **2007**, 450, 1235–1239.

(20) Sha, M. Y.; Xu, H.; Natan, M. J.; Cromer, R. *J. Am. Chem. Soc.* **2008**, 130, 17214–17215.

for further analyses.<sup>21,22</sup> All of the above highlight the importance of developing nondestructive methods for the sensitive detection of circulating tumor cells in blood samples. For our studies, we decided to use a small molecule as opposed to an antibody, because its small size could guarantee higher nanoparticle multivalency and its stability would lead to the development of robust field-deployable nanosensors that are not susceptible to thermal denaturation. As a model small molecule ligand, we chose folic acid (folate), which is the canonical affinity ligand of the folate receptor (FR) that is overexpressed in some tumor cells.<sup>23</sup> Although circulating tumor cells more prevalently overexpress other cell surface markers, such as EpCAM,<sup>19</sup> recent studies indicate that the folate receptor (FR) is overexpressed in numerous cancers, including ovarian, testicular, breast and lung.<sup>23</sup> Furthermore, as the expression of FR is upregulated during metastasis, this receptor is a good marker for diagnosis, targeted imaging and drug delivery. As our cellular target, we used A549 lung cancer cells, as lung cancer is among the most common sites of origin of metastatic cancer through migration of lung cancer cells via the circulation,<sup>24</sup> and this cell line is known to overexpress the folate receptor.<sup>23</sup> Therefore, we investigated if the folate nanoparticle preparations, and particularly the high-folate ones, can be used for the quantification and sensitive detection of single FR-expressing A549 cells in complex media, via magnetic relaxation. Results showed that low valency nanoparticles at low target concentrations induced high  $\Delta T_2$ , whereas at high cell concentrations the nanoparticles switched to a dispersed-like state with lower  $\Delta T_2$  values. Corresponding dynamic light scattering (DLS) analysis and cell-associated fluorescence studies confirmed these results. On the other hand, high valency nanoparticles from a dispersed-like state switched to a clustered state, when we increased the cell concentration. Similar observations were made when we used low and high valency nanoparticles for the detection of bacterial cells, indicating that the interaction was modulated by the nanoparticle valency and not the targeted cell's size. Furthermore, results show that the high valency nanoparticles performed better than their low valency counterparts as they achieve a high sensitivity, faster detection kinetics and more efficient magnetic isolation of cells for subsequent analyses. Hence, considering the need for circulating cancer cell diagnostic modalities, herein we demonstrate that multivalent iron oxide nanosensors, carrying a small affinity ligand, can facilitate (i) fast detection of tumor cells in blood via magnetic relaxation, (ii) the magnetic isolation and propagation of these cells for further analyses, and (iii) the cells' colorimetric identification via the nanoparticles' intrinsic peroxidase activity. The same approach can be expanded to the detection of other cells in circulation, as well as pathogens.

## Experimental Section

**Materials.** All reagents were of AR (Analytical Reagent) grade. Iron salts ( $\text{FeCl}_2 \cdot 4\text{H}_2\text{O}$  and  $\text{FeCl}_3 \cdot 6\text{H}_2\text{O}$ ) were obtained from Fluka.

- (21) Bauer, K. D.; de la Torre-Bueno, J.; Diel, I. J.; Hawes, D.; Decker, W. J.; Priddy, C.; Bossy, B.; Ludmann, S.; Yamamoto, K.; Masih, A. S.; Espinoza, F. P.; Harrington, D. S. *Clin. Cancer Res.* **2000**, *6*, 3552–3559.
- (22) Kraeft, S. K.; Ladanyi, A.; Galiger, K.; Herlitz, A.; Sher, A. C.; Bergsrud, D. E.; Even, G.; Brunelle, S.; Harris, L.; Salgia, R.; Dahl, T.; Kesterson, J.; Chen, L. B. *Clin. Cancer Res.* **2004**, *10*, 3020–3028.
- (23) Parker, N.; Turk, M. J.; Westrick, E.; Lewis, J. D.; Low, P. S.; Leamon, C. P. *Anal. Biochem.* **2005**, *338*, 284–293.
- (24) Alix-Panabieres, C.; Riethdorf, S.; Pantel, K. *Clin. Cancer Res.* **2008**, *14*, 5013–5021.

Polyacrylic acid (MW 1.8 kDa), ammonium hydroxide, hydrochloric acid, folic acid, *N,N'*-dimethylformamide (DMF), *N*-hydroxysuccinimide (NHS) and 3-(4,5-Dimethylthiazol-2-yl)-2,5-diphenyltetrazolium bromide (MTT) were purchased from Sigma-Aldrich. The dialkylcarbocyanine fluorophore DiI (D282) and the nuclear stain DAPI (4',6-diamidino-2-phenylindole - D1306) were purchased from Invitrogen. EDC (1-Ethyl-3-[3-dimethylaminopropyl] carbodiimide hydrochloride) and Protein G were obtained from Pierce Biotechnology, whereas the polyclonal rabbit anti-human folate receptor antibody (FL-257) was purchased from Santa Cruz Biotechnology. The polyclonal anti-MAP antibody was a gift from Dr. Saleh Naser (Burnett School of Biomedical Sciences, College of Medicine, UCF).

**Synthesis of Propargylated Polyacrylic-Acid-Coated Iron Oxide Nanoparticles.** The polyacrylic-acid-coated iron oxide nanoparticles were synthesized using the alkaline precipitation method, as recently reported.<sup>25</sup> Briefly, the nanoparticles were prepared by rapidly mixing a  $\text{Fe}^{3+}/\text{Fe}^{2+}$  solution with an ammonium hydroxide solution for 30 s, before adding the polyacrylic acid (PAA) solution. The nanoparticles were washed, concentrated and finally reconstituted in phosphate buffered saline (pH = 7.4), using a KrosFlo Research II TFF system equipped with a 10 kDa column (Spectrum Laboratories). Propargylation of the as synthesized nanoparticles was achieved with carbodiimide chemistry, as previously reported.<sup>25</sup> The propargylated nanoparticles were magnetically separated and characterized, following published protocols.<sup>25</sup>

**Synthesis of Folate-Carrying Nanoparticles with Different Nanoparticle Valency Using “Click” Chemistry.** To synthesize folate-conjugated nanoparticles, propargylated nanoparticles (13 mg, 1.69 mg/mL) were added to azide-functionalized folic acid (folate  $\sim \text{N}_3$ ), according to the literature.<sup>25</sup> Different levels of nanoparticle valency were achieved by varying the stoichiometric ratio of nanoparticle ligand to nanoparticle concentration. For the preparation of low-folate nanoparticles, 0.4  $\mu\text{g}$  of folic acid ( $0.8 \times 10^{-2}$   $\mu\text{mol}$ ) were used, whereas for the high-folate nanoparticles 4 mg ( $8 \times 10^{-2}$  mmol) of folic acid in DMSO. The reaction was initiated at room temperature in the presence of catalytic amount of CuI (0.01  $\mu\text{g}$ ,  $0.6 \times 10^{-10}$  mmol), in 125  $\mu\text{L}$  of bicarbonate buffer (pH 8.5), and further incubated for 12 h at room temperature (“click” chemistry). The final reaction mixture was purified with a magnetic column, and finally dialyzed using a 6000–8000 MW cutoff dialysis bag, against deionized water and phosphate buffered saline (PBS). The folate nanoparticle preparations were stored at 4 °C until further use. Confirmation of the successful conjugation of folate to the nanoparticles was achieved through UV-vis and fluorescence emission spectroscopy. To make our nanoparticles multimodal, we loaded them with a lipophilic fluorophore. Dye-doped folate-conjugated iron oxide nanoparticles were prepared by the dropwise addition of DiI (0.1  $\mu\text{g}/\mu\text{L}$  in DMF) in 4.5 mL of the nanoparticle suspension ( $[\text{Fe}] = 1.69$  mg/mL), as described in the literature.<sup>25</sup> The nanoparticles were magnetically separated, and the complete removal of free (nonencapsulated) dye was confirmed through fluorescence emission spectroscopy, demonstrating a single red-shifted emission maximum. Finally, the nanoparticles were stored in dark at 4 °C until further use.

**Synthesis of Antibody-Carrying Nanoparticles with Different Nanoparticle Valency.** For the conjugation of Protein G to the nanoparticles, polyacrylic-acid-coated nanoparticles ( $[\text{Fe}] = 0.25$  mg/mL) were taken in 2 mL MES buffer (pH = 6), and to this we added EDC (1 mg, 0.11 mmol) and NHS (0.8 mg, 0.15 mmol). This reaction mixture was incubated for 3 min, followed by dropwise addition of Protein G (1.5 mg, 60  $\mu\text{mol}$ ) in DI water (0.5 mL). Next, the solution was incubated for 30 min at room temperature under continuous mixing, followed by overnight incubation at 4 °C. To remove any Protein G molecules that did not conjugate to the nanoparticles, we performed magnetic separa-

- (25) Santra, S.; Kaittanis, C.; Grimm, J.; Perez, J. M. *Small* **2009**, 1862–1868.



tion using a 1×-PBS-equilibrated LS25 column. Protein quantification revealed that the nanoparticle preparation's Protein G concentration was 0.1  $\mu\text{g}/\mu\text{L}$ . Subsequently, we conjugated either anti-FR or anti-MAP antibodies to the Protein G-carrying nanoparticles, as previously reported.<sup>16</sup> However, to engineer the nanoparticle valency, the Protein G nanoparticles (250  $\mu\text{L}$ ) were incubated with different antibody amounts (5  $\mu\text{g}$  anti-FR, 0.5 ng anti-FR, 5  $\mu\text{g}$  anti-MAP or 0.5 ng anti-MAP), yielding either anti-FR or anti-MAP nanoparticles with different degrees of valency, which was assessed in accordance to the literature.<sup>26,27</sup>

**Nanoparticle Characterization.** The size of the folate-conjugated iron oxide nanoparticles was determined through dynamic light scattering (DLS), using a PDDLS CoolBatch 40T instrument and the Precision Deconvolve 32 software. Iron concentration was determined spectrophotometrically after acid digestion of the nanoparticles' suspension as previously reported,<sup>25,28</sup> whereas  $r_1$  and  $r_2$  relaxivity measurements were obtained using a 0.47T mq20 NMR analyzer (Minispec, Bruker, Germany). Zeta potential measurements were performed on a Nano-Z zetasizer (Malvern), operating at 25 °C. To determine the presence of propargyl groups on the surface of the propargylated nanoparticles, FT-IR was performed on a PerkinElmer Spectrum 100 FT-IR spectrometer, and to confirm the successful conjugation of folate to the folate nanoparticles' surface UV-vis absorbance and fluorescence emission profiles were obtained, using a Cary300 spectrophotometer (Varian) and a NanoLog-3 fluorimeter (Horiba Jobin-Yvon). Similarly, the folate nanoparticles' fluorescence emission associated with the encapsulated DiI was determined with the NanoLog-3 fluorimeter. Protein G and antibody quantification was achieved colorimetrically through the BCA assay (Pierce) in accordance to the supplier's protocol, and determination of the amount of folate and antibody per nanoparticle was determined as described in literature.<sup>16,26,27</sup>

**Mammalian Cell Studies. Cell Cultures.** Cancer human alveolar cells (A549) and normal (noncancer) rat cardiomyocytes (H9c2) were obtained from ATCC, and maintained in accordance to the supplier's protocols. Briefly, the A549 cells were maintained in a 5%-FBS-containing DMEM medium supplemented with antimycotic/antibiotic, whereas the H9c2 cells were propagated in a 10%-FBS-containing MEM medium containing antimycotic/antibiotic. All cell cultures were grown in a humidified incubator at 37 °C under a 5% CO<sub>2</sub> atmosphere.

**Hemocytometer-Mediated Cell Quantification.** After detaching the cells from the culture plate using trypsin and suspending them in growing medium, the cellular suspension was centrifuged at 1000 rpm for 8 min and the pellet was resuspended in 2 mL of the corresponding medium. Ten microliter aliquots of the resulting cell suspensions were thoroughly mixed with 10  $\mu\text{L}$  trypan blue solutions. Quantification was performed using a hemocytometer and a phase-contrast microscope.

**Serial Dilutions of Stock Cellular Suspensions.** After determining the cell concentration of the stock suspensions, serial dilutions were prepared in 1× PBS, 5% PBS-diluted blood or whole blood, using aseptic techniques. Fresh blood was a gift from Dr. James Hickman (UCF NSTC), obtained from bacteremia-free Crl:CD-(SD)IGSBR female rats (Charles River Laboratories). All serial diluted samples were used immediately after preparation.

**Fluorimetry-Based Determination of Nanoparticles-Cell Association.** One milliliter cellular suspensions (10<sup>3</sup> and 10<sup>6</sup> A549 cells) in PBS, were incubated with 1  $\mu\text{L}$  of folate-carrying nanoparticles ([Fe] = 1.69  $\mu\text{g}/\text{mL}$ ) for 60 min at room temperature, under continuous mixing (300 rpm). To remove any unbound nanoparticles, the samples were centrifuged three times at 1000

rpm for 8 min, each centrifugation round followed by washing with 1× PBS. The resulting cell pellets were resuspended in 1 mL of 1× PBS, and fluorescence emission spectra were recorded using a NanoLog-3 fluorimeter (Horiba Jobin-Yvon).

**Confocal Laser-Scanning Microscopy.** A549 cells were grown overnight on culture dishes, before treatment. After incubation with the nanoparticles, the cells were washed three times with 1× PBS, fixed with 5% formalin solution, and stained with DAPI (Molecular Probes). Subsequently, the cells were examined with a Zeiss LSM 510 confocal microscope equipped with a 40X objective.

**Dynamic Light Scattering (DLS).** One mL cellular suspensions in PBS, either with 10<sup>3</sup> or 10<sup>6</sup> A549 cells, were incubated with 1  $\mu\text{L}$  folate-PAA-IONP ([Fe] = 1.69  $\mu\text{g}/\text{mL}$ ) for 60 min at room temperature, under continuous mixing (300 rpm). The alterations in the nanoparticle size distribution were monitored through the PDDLS CoolBatch 40T instrument and the Precision Deconvolve 32 software.

**Magnetic-Relaxation-Mediated Cell Detection.** Ten  $\mu\text{L}$  aliquots of cell suspensions were incubated with 190  $\mu\text{L}$  of nanoparticle working solutions ([Fe] = 0.01  $\mu\text{g}/\mu\text{L}$ ) at room temperature. Spin-spin relaxation times ( $T_2$ ) were recorded over time via the 0.47T mq20 NMR analyzer (Minispec, Bruker, Germany), operating at 40 °C.

**Magnetic Isolation of A549 Cells and Detection of the Expression of the Folate Receptor.** After screening samples via magnetic relaxation, they were incubated with various concentrations of folate-PAA-IONP for 30 min at 37 °C. Subsequently, each sample was passed through a 1×-PBS-equilibrated LS25 MACS column (Miltenyi Biotec). After removing the column from the magnet, the eluate was captured in culture dishes with 5%-FBS-containing DMEM medium. The dishes were placed in a humidified incubator (37 °C, 5% CO<sub>2</sub>) for 24 h, as according to the supplier the doubling time of A549 cells is 18 h. Then, the cells were washed three times with 1× PBS and fresh medium was added. Cells were quantified using the hemocytometer method and 500-cell aliquots of either A549 or H9c2 cells were seeded into a 96-well microtiter plate. After overnight growth, the cells were incubated for 1 h with different nanoparticle concentrations at 4 °C. Then, the cells were washed three times with 1× PBS in order to remove any unbound nanoparticles, and 100  $\mu\text{L}$  of 0.2 mM TMB in citrate buffer pH 4.0 (3, 3', 5, 5'-tetramethylbenzidine, Sigma) as well as 10  $\mu\text{L}$  H<sub>2</sub>O<sub>2</sub> (Acros) were added. Twenty minutes after, absorbance was recorded at 652 nm, using a  $\mu\text{Quant}$  200 microtiter plate reader (Biotek).

**Flow Cytometry.** A549 and H9c2 cells were grown until reaching confluence. After detachment and centrifugation at 1000 rpm, the cell pellets were collected and resuspended in 1× PBS. The resulting cell suspensions were incubated with the anti-folate-receptor antibody (0.5  $\mu\text{g}/\text{mL}$ ) for 30 min at 4 °C, under continuous mixing. After the incubation with the primary antibody, the cells were centrifuged and resuspended in PBS three times, followed by a 30-min incubation at 4 °C with an FITC-conjugated goat anti-rabbit-IgG antibody (0.5  $\mu\text{g}/\text{mL}$ ). The FITC-conjugated antibody was a gift from Dr. James Hickman (Nanoscience Technology Center, UCF). Finally, the cells were centrifuged and resuspended in PBS three times, and the cellular suspensions were examined using a FACSCalibur flow cytometer (BD Biosciences).

**Cell Viability Studies.** Equal populations of A549 cells, either magnetically isolated using the folate-carrying iron oxide nanoparticles or readily harvested, which had been quantified with a hemocytometer, were seeded in 96-well plates. After overnight growth in a 5%-FBS-containing DMEM medium at 37 °C, 5% CO<sub>2</sub> in a humidified incubator, the cells were washed three times with 1× PBS and treated with 20  $\mu\text{L}$  MTT (5  $\mu\text{g}/\mu\text{L}$ , Sigma-Aldrich) for 2 h. Using acidified isopropanol (0.1 N HCl), the formazan crystals were dissolved and the absorbance was recorded at 570 and 750 nm (background) via a Synergy  $\mu\text{Quant}$  microtiter plate reader (Biotek).

**Bacterial Cell Studies. Bacterial Stocks.** Serial dilutions of heat inactivated *Mycobacterium avium* ssp. *paratuberculosis* (MAP) in

(26) Koch, A. M.; Reynolds, F.; Kircher, M. F.; Merkle, H. P.; Weissleder, R.; Josephson, L. *Bioconjug Chem* **2003**, *14*, 1115–1121.

(27) Shen, T.; Weissleder, R.; Papisov, M.; Bogdanov, A., Jr.; Brady, T. J. *Magn Reson Med* **1993**, *29*, 599–604.

(28) Nath, S.; Kaitanis, C.; Ramachandran, V.; Dalal, N. S.; Perez, J. M. *Chem. Mater.* **2009**, *21*, 1761–1767.

1 × PBS and anti-MAP antibody were a gift from Dr. Saleh Naser (Burnett School of Biomedical Sciences, College of Medicine, UCF).

**Magnetic-Relaxation-Mediated Bacterial Cell Detection.** Similar to the mammalian cell (A549) protocol, 10 μL aliquots of cell suspensions were incubated with 190 μL of nanoparticle working solutions ([Fe] = 0.01 μg/μL) at room temperature. Spin–spin relaxation times ( $T_2$ ) were recorded over time via the 0.47T mq20 NMR analyzer (Minispec, Bruker, Germany), operating at 40 °C.

**Dynamic Light Scattering (DLS).** Similar to the corresponding mammalian studies, one mL MAP bacterial suspensions in PBS, either with 500 or 5 CFUs (Colony Forming Units), were incubated with 1 μL anti-MAP-PAA-IOPN ([Fe] = 0.50 μg/mL) for 60 min at room temperature, under continuous mixing (300 rpm). The alterations in the nanoparticle size distribution were monitored through the PDDLS CoolBatch 40T instrument and the Precision Deconvolve 32 software.

**Data Analysis.** All experiments were performed at least three times, and during each experiment three measurements were taken for each experimental condition. Each graph data set contains the obtained averages of the corresponding study. Total fluorescence intensity per mL (Total FI<sub>mL</sub>) is defined as the summation of each 1-mL sample's fluorescence intensities from 570 to 640 nm. For the magnetic relaxation quantification plots, the best model fit was achieved using either linear or sigmoidal fit (OriginPro 7.5, Origin Lab Corp, MA). As we previously reported,  $\Delta T_2$  is defined as the average  $T_{2, \text{sample}, i}$  minus the average  $T_{2, \text{control}, i}$  at time  $i$ , where for the control sample sterile, nonspiked medium (blood or milk) was used.<sup>17</sup> To determine cell viability, we subtracted the background absorbance at 750 nm from the absorbance at 570 nm, as previously reported.<sup>25</sup> The percentage cell viability for the cells isolated was calculated using the formula:  $\Delta A_{570-750 \text{ sample}} / \Delta A_{570-750 \text{ control}} \times 100$ , where the corresponding control for the cells isolated with low- and high-folate nanoparticles were harvested cells seeded in low and high population counts (Control low and Control high).

## Results

**Synthesis of Iron Oxide Nanoparticles with Ligand-Varying Valency.** To examine our hypothesis, we prepared polyacrylic-acid-coated iron oxide nanoparticles with different ligand valency by varying the stoichiometry of the conjugation reaction. These polymer-coated nanoparticles had an average hydrodynamic diameter of 90 nm,  $\zeta$  potential of  $-82.6 \pm 2.4$  mV, spin–lattice ( $r_1$ ) and spin–spin relaxations ( $r_2$ ) of  $53 \text{ mM}^{-1} \text{ s}^{-1}$  and  $206 \text{ mM}^{-1} \text{ s}^{-1}$ , respectively. “Click” conjugation of targeting moieties to the nanoparticles' surface was achieved by incorporating alkyne groups via carbodiimide chemistry (Supporting Information (SI) Scheme 1 and SI Figure 1), having a  $\zeta$  potential of  $-62.6 \pm 2.9$  mV. As a model targeting moiety, we used folic acid (MW 441.4 kDa), which is the affinity ligand of the transmembrane folic acid receptor (FR) that is overexpressed in several cancers.<sup>23</sup> Hence, azide-functionalized folic acid was conjugated to the alkyne-carrying polyacrylic-acid-coated nanoparticles via click chemistry, having different concentrations of folate while maintaining constant the nanoparticle concentration. The presence of folate on the nanoparticles was corroborated by the presence of a 352 nm shoulder in the UV–vis absorbance spectrum (SI Figure 2) and a corresponding 446 nm band in the fluorescence emission spectrum (SI Figure 3). Using this spectrophotometric information and following published protocols,<sup>26,27</sup> we determined that the high-folate nanoparticles had on average 120 folic acid moieties per nanoparticle ( $\zeta$  potential =  $-59.4 \pm 3.6$  mV), whereas the low-folate nanoparticles had on average 1 folic acid per nanoparticle ( $\zeta$  potential =  $-53.5 \pm 4.1$  mV). The folate-carrying nanoparticles were then doped with the fluorophore (DiI), resulting in fluorescently labeled

nanoparticles (SI Figure 4), as recently reported.<sup>25</sup> Contrary to fluorophore conjugation to the nanoparticles' surface, this method facilitates fluorophore encapsulation within the polymeric coating's microdomains and does not compromise the nanoparticles' folic acid valency, allowing the use of these nanoparticles in fluorimetric (Figure 1) and confocal microscopy studies with folate-receptor expressing cells (SI Figure 5).

In addition to the folate nanoparticles that carry a small molecule (folate), we synthesized nanoparticles with different levels of anti-folate-receptor (anti-FR) antibodies (MW 150 000 kDa). Specifically, via carbodiimide chemistry, Protein G was conjugated to the as synthesized polyacrylic-acid-coated nanoparticles, which have readily available carboxylic acid groups. Following magnetic separation and nanoparticle-associated protein quantification (2 Protein G molecules per nanoparticle on average), the antibodies were conjugated to the Protein G nanoparticles through an overnight reaction carried out at 4 °C. Specifically to engineer the valency and obtain nanoparticles with either low or high levels of conjugated antibodies, we varied the stoichiometry of the nanoparticle conjugation reaction, by modifying one of the reactant's concentration (either 5 μg anti-FR or 0.5 ng anti-FR) while keeping the Protein G nanoparticles' amount constant (250 μL). These conjugation reactions resulted in the formation of nanoparticles with high (4 anti-FR molecules per nanoparticle on average) and low (1 anti-FR molecule per nanoparticle on average) anti-FR levels, as determined with the BCA assay following literature available protocols.

**Assessment of the Ligand-Modulated Nanoparticle–Mammalian Cell Interactions.** To test our hypothesis, we first investigated the nanoparticle–cell associations via fluorescence spectroscopy. Since our nanoparticles apart from magnetic are fluorescent, we employed this technique due to its enhanced sensitivity and spectral acquisition capability, allowing the determination of the nanoparticle–cell association and quantification of this interaction by recording the fluorescence emission from the magnetically isolated folate-receptor expressing cells. Therefore, any fluorescence emission associated with the isolated cells should have been an indication of the degree of interaction between the nanoparticles' ligands and cell surface receptors. A major advantage of fluorescence spectroscopy in contrast to confocal laser scanning microscopy is its ability to determine the cell–nanoparticle interaction in suspension, where confocal microscopy requires adherent cells. Additionally, although flow cytometry is an alternative solution-based technique, it was not employed because (i) large cell populations are required to obtain statistically significant results, (ii) it has limited sensitivity for fluorophores that weakly associate with cells or at low fluorophore concentrations (for instance few nanoparticles), and (iii) the compromised multispectral capability (restricted number of acquired wavelengths).

Thus for the fluorimetry studies, the two nanoparticle preparations having different folate levels (120 versus 1 folate molecule per nanoparticle) were incubated for 1 h at room temperature under constant mixing with folate-receptor-expressing lung carcinoma cells (A549) in suspension,<sup>23</sup> followed by cell harvesting via centrifugation. The resulting cell pellets were washed with 1 × PBS to remove any unbound nanoparticles and finally reconstituted in 1 mL 1 × PBS, allowing the comparison of total fluorescence emission per mL (total FI<sub>mL</sub>) among the various samples. Interestingly, fluorimetry studies revealed that the total fluorescence emission from the low cell density sample incubated with low-folate nanoparticles was higher than that

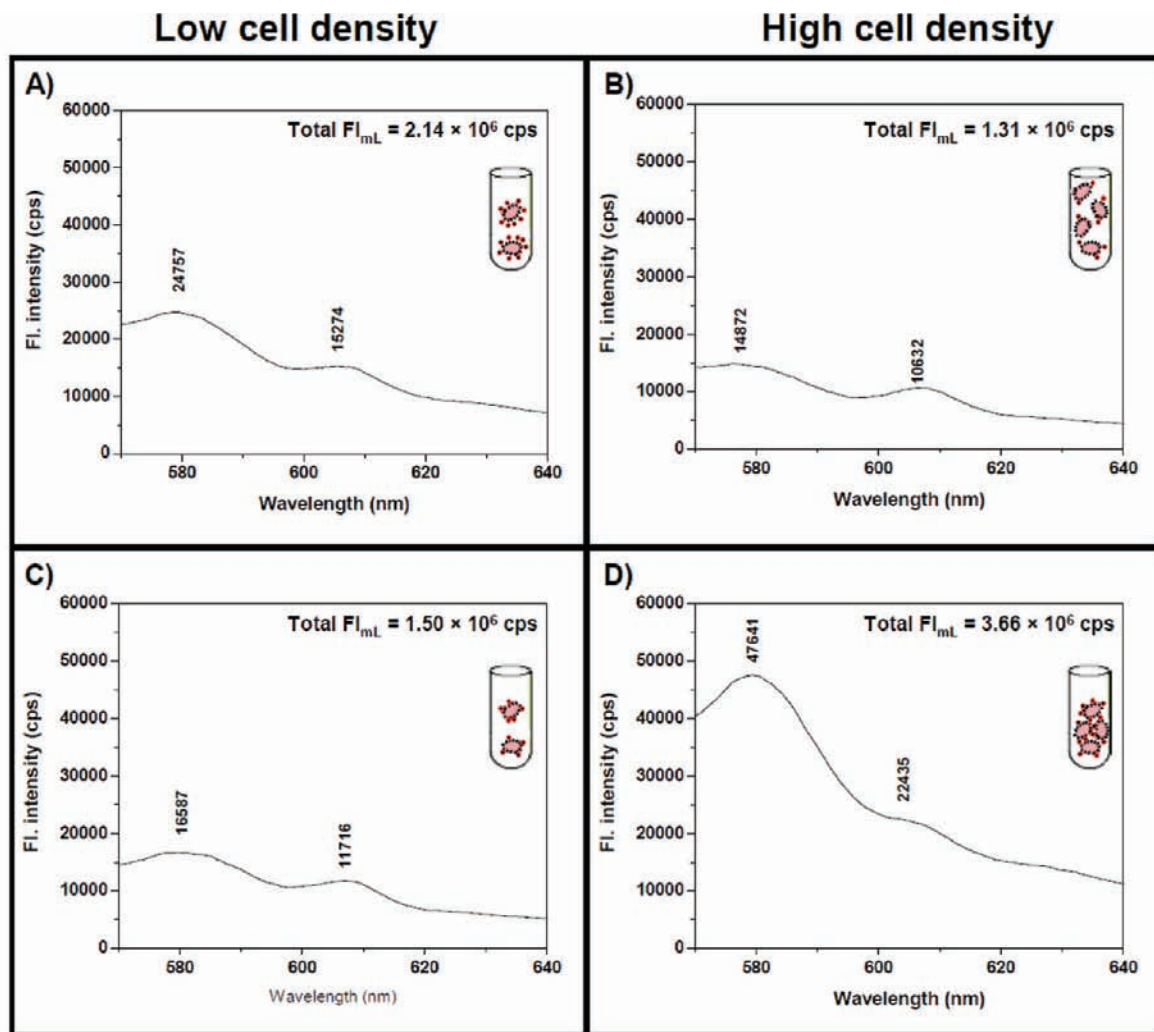


**Figure 1.** Distinct associations between fluorescent-labeled folate iron oxide nanoparticles and FR-expressing cells (A549) due to the nanoparticles' different valency. (A) Low and (B) high cell density A549 cells incubated with DiI-encapsulating low-folate nanoparticles. (C) Low and (D) high cell density A549 cells incubated with the corresponding high-folate nanoparticles. (The two primary fluorescence emission peaks for DiI are indicated, as well as the total fluorescence emission of the acquired spectra. Insets diagrammatically represent the interactions between cells and the nanoparticles in equal-volume samples.)



of the corresponding high cell density sample (Figure 1A and B). This difference may be attributed to the higher number of recognizable epitopes in the cell suspension, as a result of the higher cell density (more cells more folate receptors), mediating the nanoparticles' quasi-dispersion with a concomitant reduction in cell-associated fluorescence.

Likewise, we assessed the high-folate nanoparticles interaction with A549 cells, by employing the same experimental approach. Contrary to what was observed with the low-folate nanoparticles, fluorimetry studies demonstrated that under conditions of low cell density, the total fluorescence emission was lower than that from the high cell density sample (Figure 1C and D). It is plausible that at low cell density the nanoparticles' higher valency may have facilitated the interaction of a given nanoparticle with multiple folate receptors found on the same cell. Consequently, this may have caused fewer high-folate nanoparticles interacting with a given cell, leading to less prominent cell-associated fluorescence. However, under high cell density, the high-folate nanoparticles multivalency could have promoted the nanoparticle's intercellular interaction with folate receptor epitopes found on adjacent cells in the nanoparticle's proximity, leading to enhanced fluorescence emission.

To further assess the interaction between our nanoparticles and cells, DLS was used to determine how the nanoparticle valency differentially mediates the dispersion state of the nanoparticles in solution under varying target cancer cell concentrations. In the absence of any cell in solution, the nanoparticles were highly dispersed as 100% of the nanoparticles had a diameter below 100 nm, as previously reported.<sup>25</sup> When the low folate nanoparticles were added to a suspension of cells at low cell density ( $10^3$  A549 cells/mL), 23% of these nanoparticles formed large nanoparticle aggregates while only 77% remained dispersed (Table 1). In contrast, only 14% of the high-folate nanoparticles formed nanoparticle aggregates at the same cell density ( $10^3$  A549 cells/mL), in accordance with our hypothesis (Table 1). As stated before, this may be attributed to the fact that the high-folate nanoparticles' increased valency can facilitate the interaction of a nanoparticle with multiple target receptors on the same cell, similar to what was observed through fluorescence spectroscopy (Figure 1C). Interestingly, when we increased the number of cells in suspension to  $10^6$  cells/mL, the population of low-folate nanoparticles adopting a clustered state decreased from 23 to 13%, whereas the population of clustered high-folate nanoparticles increased from 14% to 35%



**Table 1.** Size Distribution of the Folate Nanoparticles in the Presence of Various A549 Concentrations (Means  $\pm$  SE)

Nanoparticle	Diameter (nm)	Cell density	
		Low	High
	> 100	23 $\pm$ 0.4%	13 $\pm$ 0.5%
	< 100	77 $\pm$ 0.3%	87 $\pm$ 0.2%
	>100	14 $\pm$ 0.2%	35 $\pm$ 0.3%
	< 100	86 $\pm$ 0.3%	65 $\pm$ 0.5%

(Table 1). These changes are in line with the fluorimetry data, where similar changes were observed. Specifically, for the low-folate nanoparticles, DLS indicated a reduction by a factor of 1.77 versus 1.63 by fluorescence spectroscopy, whereas for the high-folate nanoparticles both methods provided comparable results (a factor of 2.5 by DLS vs 2.43 by fluorimetry). Taken together, the fluorimetry and dynamic light scattering results corroborate our model, and demonstrate that the nanoparticles' ligand valency modulates the differential interactions between folate nanoparticles. Hence, these distinct nanoparticle–cell associations in solution may facilitate different magnetic relaxation sensing dynamics and cell capturing capabilities.

**Role of the Nanoparticle Valency in Magnetic-Relaxation-Mediated Mammalian Cell Detection.** Detection with magnetic relaxation nanosensors (MRnS) is governed by the degree of nanoparticle association with a target.<sup>15,16</sup> Based on the aforementioned data, we reasoned that there would be dramatic differences in the magnetic-relaxation-mediated cell detection, attributed to the nanoparticles' valency. We anticipated that nanoparticles with high valency, due to the multiple specific interactions between their carrying ligands and cell epitopes, may achieve better detection sensitivity and even single cancer cell quantification. This is critical, as it was recently demonstrated that even a single metastatic cancer progenitor cell can successfully induce tumor formation.<sup>29</sup>

Specifically, we utilized the folate nanoparticle preparations (1 versus 120 folate moieties per nanoparticle) and the anti-FR ones (1 versus 4 antibody molecules per nanoparticle) to assess the detection performance of these nanosensors. To demonstrate the potential ability of our nanosensors to detect circulating cancer cells in clinical samples, we detected A549 cells in blood diluted in phosphate buffered saline (PBS). In these studies, a stock cellular suspension of A549 cells was quantified using a hemocytometer, followed by the preparation of serial dilutions of the stock suspension in PBS-diluted blood. Subsequently, 10  $\mu$ L aliquots of the resulting cellular suspensions were incubated with 190  $\mu$ L of the corresponding nanoparticle working solution ( $[\text{Fe}] = 0.01 \mu\text{g}/\mu\text{L}$ ) at room temperature, while monitoring the changes in spin–spin relaxation ( $\Delta T_2$ ) with a magnetic relaxometer operating at 0.47 T.

After a brief 1-h-long incubation at room temperature under continuous mixing, distinct valency-dependent trends were observed (Figure 2A–D). We chose 1-h-long incubation at room temperature in order to investigate the field applicability of our assay and its ability to provide fast and reliable results, whereas

mixing of the samples minimized the possibility of nanoparticle internalization via folate-receptor-mediated endocytic uptake. An increase in the  $\Delta T_2$  was observed as the number of A549 lung carcinoma cells increased in solution when both high valency nanoparticles (high folate and high anti-FR antibody) were used (Figure 2A and B), whereas the opposite trend was observed for the nanoparticles with low ligand levels on their surface (decrease in  $\Delta T_2$  when the cell concentration increased) (Figure 2C and D). These results supported our hypothesis and were in line with the DLS and fluorimetry data. Specifically, as the  $\Delta T_2$  for high cell counts (>1000) of the low-folate nanoparticles was 1.5–1.7 ms and the  $\Delta T_2$  for a single cell detected by the high-folate nanoparticles was 2.5 ms, this may be attributed to the fact that 13% of the low folate nanoparticles interacted with cells at high cell density versus 14% of the high valency nanoparticles associated with cells at low cell density, as determined through DLS (Table 1).

Furthermore, our data suggest that in our previous report<sup>17</sup> the observed decrease in  $\Delta T_2$  upon increase of the bacteria concentration was attributed to the nanoparticles' low antibody levels (low nanoparticle valency). This is corroborated by the detection pattern of the low-anti-FR nanoparticles (Figure 2D), exhibiting sigmoidal shape similar to our previous report using MAP bacteria and a corresponding low valency nanoparticle.<sup>17</sup> Although the detection threshold of the low valency anti-FR nanoparticles was  $10^4$  cells, the low-folate nanoparticles were more sensitive and able to detect a single cell and quantify the target within the range of 1 to  $10^3$  cells, (Figures 2C). Most importantly, the high-folate nanoparticles were able to detect and quantify cells within an even wider dynamic range ( $1 - 10^6$ ) (Figures 2A), outperforming the high anti-FR nanoparticles (Figures 2B) and demonstrating the versatility of small molecule ligands. Performing the magnetic relaxation studies at shorter incubation times (15 min) compromised data quality for the low-folate and both anti-FR nanoparticle preparations, leading to poor correlation coefficients (SI Table 1). However, the high-folate nanoparticles achieved good correlation coefficients ( $R^2 > 0.9$ ) even after a 15-min incubation, demonstrating the enhanced detection kinetics of the high-folate nanoparticles (Figure 3). Therefore in light of these results, valency plays a critical role in the detection profile of cancer cells using magnetic relaxation, as multivalency achieved via small molecules (folate) facilitates fast single cell detection in blood.

Next, we studied the specificity of our high-folate nanoparticles toward the folate receptor. Previously, it has been reported that antibody-carrying iron oxide nanoparticles can specifically detect bacteria,<sup>17,28</sup> whereas negative controls of Protein-G iron oxide nanoparticles yielded no changes in the relaxation times.<sup>28</sup> First, we saturated the nanoparticles' solution with excess folate (10 mg/mL), and data indicated that the folate nanoparticles could not detect the lung carcinoma cells (A549) under these conditions, as seen by the concomitant absence of significant changes between the samples screened (Figure 4A). Likewise, saturation of the culture medium with excess folate (10 mg/mL) prevented the nanoparticles' interaction with the cells' folate receptors (FR), as indicated by the absence of fluorescence emission from the plasma membrane (SI Figure 6). Furthermore, we used cells that do not express the folate receptor (H9c2),<sup>23</sup> which when incubated with the nanosensors failed to induce any cell-concentration-dependent changes in the solution's  $T_2$  times (Figure 4B). Thus, these data support the hypothesis that the folate nanoparticles interact specifically with the folate receptor at the plasma membrane of cells expressing this

(29) Quintana, E.; Shackleton, M.; Sabel, M. S.; Fullen, D. R.; Johnson, T. M.; Morrison, S. J. *Nature* **2008**, *456*, 593–598.

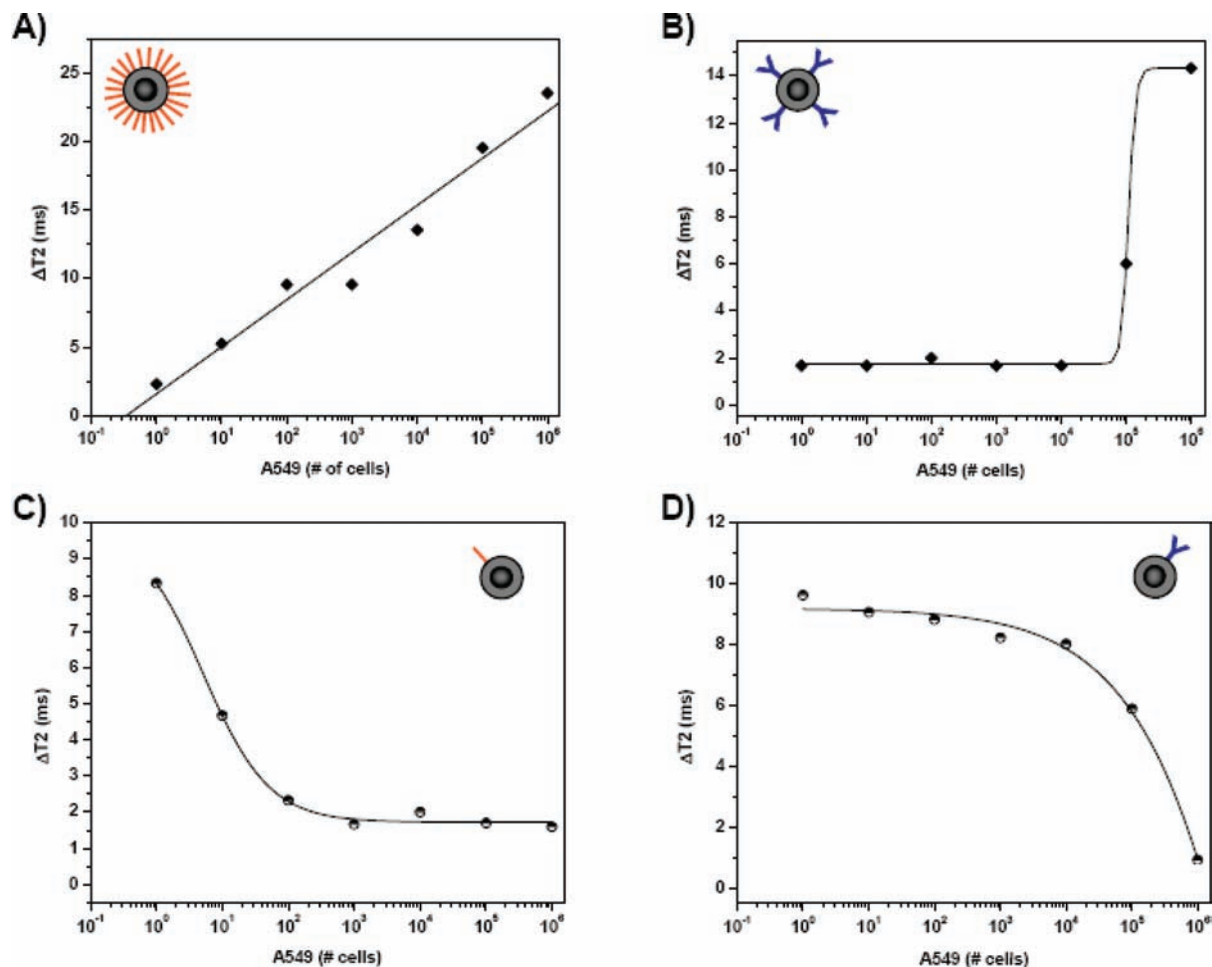


**Figure 2.** Relaxation-mediated detection of cancer cells in PBS-diluted blood after a 60-min incubation, using (A) high-folate nanoparticles, (B) high-anti-FR nanoparticles, (C) low-folate nanoparticles, and (D) low-anti-FR nanoparticles. (Means  $\pm$  SE; SE were within 1–2%, which are too small to be depicted.)

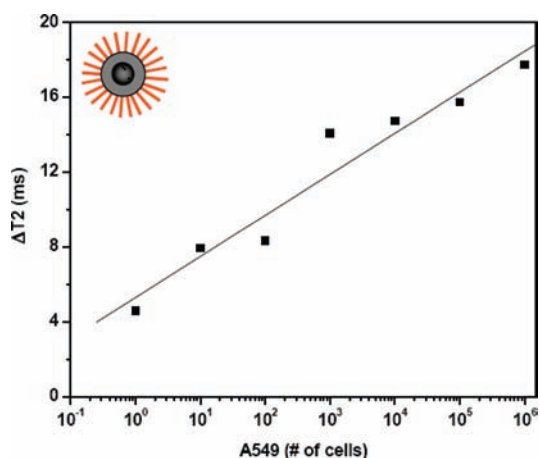


**Figure 3.** Relaxation-mediated detection of cancer cells in PBS-diluted blood after a 15-min incubation using high-folate nanoparticles. (Means  $\pm$  SE; SE were within 1–2%, which are too small to be depicted.)

receptor, facilitating magnetic relaxation detection and fluorescence imaging.

**Assessment of the Ligand-Modulated Nanoparticle–Bacterium Interactions.** After elucidating the role of nanoparticle valency in the nanoparticle–mammalian cell interaction in the target cells' magnetic relaxation detection trend and sensitivities, we investigated if this behavior applied to other systems. Particu-

larly, we examined the role of the nanoparticle valency in the detection of bacteria. Hence for these studies, *Mycobacterium avium* spp. *paratuberculosis* (MAP) was used, which is smaller than mammalian alveolar cells ( $0.3 \mu\text{m}$  Vs  $50 \mu\text{m}$ ) and has dimensions comparable to other clinical relevant pathogens. Recently, we reported the magnetic-relaxation-mediated detection of MAP in complex media, observing that at low bacterial concentrations high  $\Delta T_2$  values were obtained, whereas at high bacterial concentrations  $\Delta T_2$  decreased.<sup>17</sup> To elucidate this phenomenon, we prepared two MAP-specific nanosensors that carried different levels of anti-MAP antibodies. Specifically, two anti-MAP nanoparticle preparations with different valency levels were prepared, by varying the stoichiometric ratio of anti-MAP antibody to Protein-G nanoparticles ( $5 \mu\text{g}$  anti-MAP: $250 \mu\text{L}$  Protein-G nanoparticles Vs  $0.5 \text{ ng}$  anti-MAP: $250 \mu\text{L}$  Protein-G nanoparticles). The resulting anti-MAP nanoparticles had either high (4 anti-MAP molecules per nanoparticle on average) or low (1 anti-MAP molecule per nanoparticle on average) antibody levels per nanoparticle.

Through DLS, we observed that the anti-MAP nanoparticles yielded similar results to those obtained with the nanoparticles for the FR-expressing mammalian cancer cells (SI Table 2). Likewise, a valency-mediated differential behavior was also observed when we quantified MAP in whole milk using magnetic relaxation and the anti-MAP nanoparticle preparations, following literature available protocols.<sup>17</sup> In particular, the low-



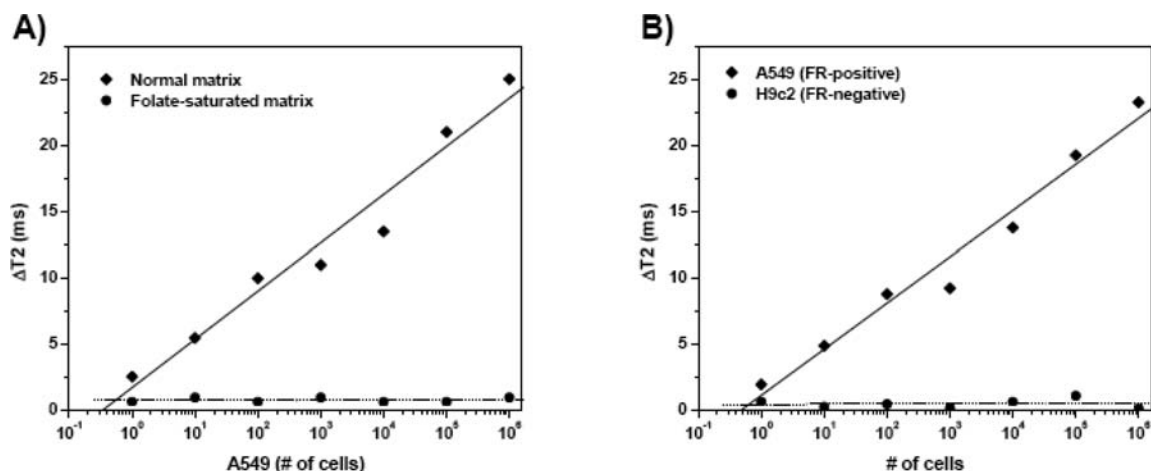


**Figure 4.** Determination of the folate nanoparticles' specificity through either (A) saturation of the matrix with excess folate or (B) folate-receptor (FR) negative cells. (Means  $\pm$  SE; SE were too small to be displayed (1–2%).)

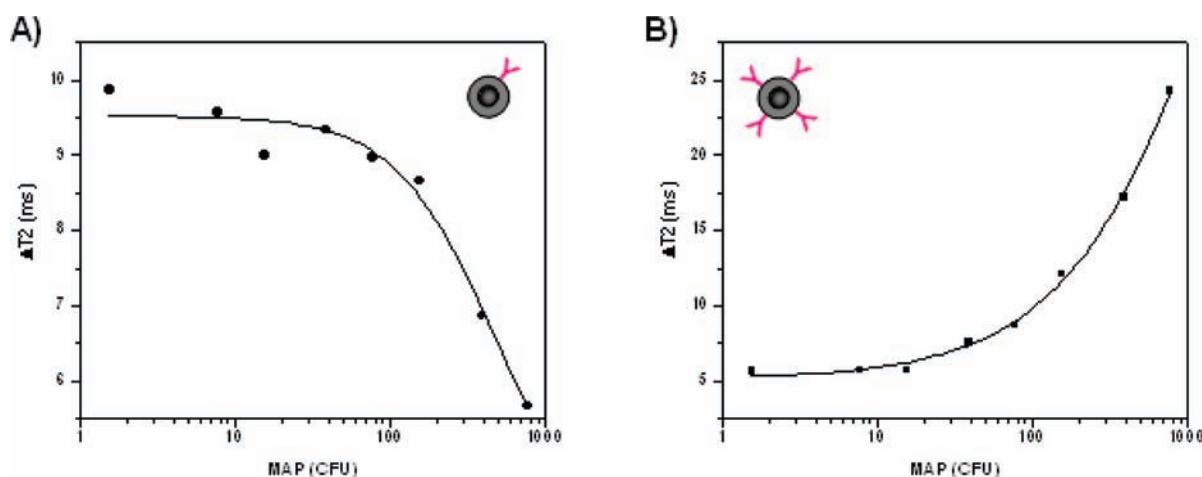


**Figure 5.** Relaxation-mediated detection of bacteria (MAP) in whole milk after a 60-min incubation at room temperature. (A) Low-anti-MAP ( $R^2 = 0.97$ ) and (B) high-anti-MAP ( $R^2 = 0.99$ ) nanoparticles. (Means  $\pm$  SE; SE was within 1–2%, which cannot be depicted.)

anti-MAP nanoparticles exhibited high  $\Delta T_2$  at low bacterial concentrations, whereas at high bacterial concentrations  $\Delta T_2$  decreased (Figure 5A). These findings were in line with the aforementioned studies using low valency nanoparticles and our earlier report on bacteria detection.<sup>17</sup> On the other hand, the high-anti-MAP nanoparticles demonstrated low  $\Delta T_2$  at low MAP concentrations, but as the target's concentration increased  $\Delta T_2$  increased (Figure 5B). Overall, the anti-FR and anti-MAP nanoparticles demonstrated similar quantifying capabilities, despite performing these studies in different matrices (blood Vs milk). Specifically, the high-anti-FR and high-anti-MAP nanoparticles can both quantify a region of 2 orders of magnitude ( $10^4$ – $10^6$  A549 cells and 10–1000 MAP CFUs respectively). Likewise, the low-anti-FR and low-anti-MAP nanoparticles can quantify roughly the same region of 2 orders of magnitude ( $10^4$ – $10^6$  A549 cells and  $\sim$ 30–1000 MAP CFUs), suggesting that this behavior may be attributed to the nature and dynamics of the antibody–antigen interaction.

Most importantly, these data suggest that the differential clustering of the nanoparticles is nanoparticle-valency-dependent, as neither the size of the ligands (small molecule Vs antibody) nor the size of the target (mammalian Vs bacterial cell) governs the interaction of the nanoparticles with a target. This is supported by the magnetic relaxation, DLS and fluorimetry data, indicating that more high-valency nanoparticles

associate with cells at high cell density, as opposed to lower cell density. If the nanoparticle size governed the interaction with cells, one would have expected comparable levels of nanoparticles associating per target regardless of cell density and no differences between the low- and high-ligand nanoparticles detection patterns. Therefore, in light of these studies, our previously reported findings on bacteria detection<sup>17</sup> were attributed to the nanoparticles' low valency. Taken together, the results of the bacterial studies corroborate what was observed with the mammalian cells (A549) and further support our hypothesis.

**The Role of the Nanoparticle Valency in the Magnetic Isolation of Cells.** MRnS detection is a nondestructive technique performed in suspensions, causing no damage to the cells. Therefore, we reasoned that after MRnS identification, cells could be magnetically isolated and used for further assays. Particularly, we hypothesized that nanoparticles with high valency would be able to magnetically isolate a higher number of cells, due to the contribution of multivalent interactions between the nanoparticles and their corresponding cellular targets. Considering the folate nanosensors' MRnS detection sensitivity and their robustness as they do not carry any heat-labile antibodies, we studied the performance of the folate nanoparticle preparations with low and high multivalency to magnetically isolate lung cancer cells with an LS25 MACS

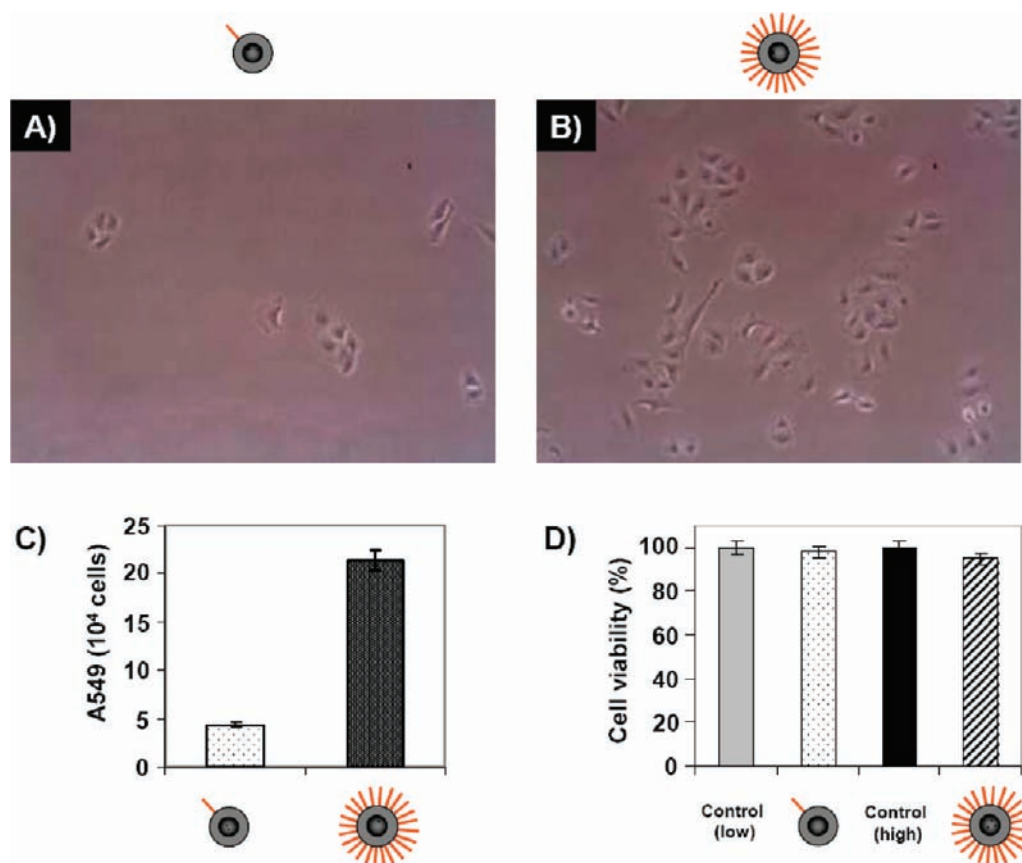


**Figure 6.** Nanoparticle-mediated magnetic isolation of FR-expressing cells. (A) Low- and (B) high-folate nanoparticles. (C) Hemocytometer-mediated quantification of the captured cells after 24 h propagation at 37 °C, 5% CO<sub>2</sub>. (D) Cell viability of cells magnetically isolated with the low- and high-folate nanoparticles (Control low –45 000 seeded cells, Control high –215 000 cells). (Means ± SE.)

column (Miltenyi Biotec). Acknowledging the need for circulating tumor cell isolation and propagation in order to use these cells for further assays,<sup>19</sup> samples of equal population A549 cells in PBS-diluted blood, which had been screened through magnetic relaxation, were effectively isolated with either the low-folate ([Fe] = 0.75  $\mu\text{g}/\mu\text{L}$ ) or high-folate nanoparticles ([Fe] = 0.75  $\mu\text{g}/\mu\text{L}$ ) and then propagated (Figure 6A and B). However, the nanoparticles with lower valency captured fewer cells than the high-folate nanoparticles, as indicated by the corresponding cell counts after a 24 h propagation at 37 °C, 5% CO<sub>2</sub> (~45 000 cells for the low-folate nanoparticles Vs ~215 000 cells for the high-folate nanoparticles) (Figure 6C). In order to assess if the magnetic isolation of the cells compromised their cell viability, we utilized the MTT assay. Results indicated that the viability of the magnetically isolated cells was comparable to that of the corresponding controls (Figure 6D), demonstrating that the magnetic-relaxation-mediated detection and magnetic isolation of cells with the folate-carrying nanoparticles is nondestructive.

Next, we determined the magnetic cell-capturing efficiency of the high-folate nanoparticles, since these magnetic nanosensors exhibited enhanced detection sensitivity through magnetic relaxation and higher magnetic isolation of cells after analysis than the low-folate nanoparticles. Hence, after relaxation-mediated detection, the cell-containing PBS-blood samples were incubated with various iron concentrations of high-folate nanoparticles and then magnetically separated. Results showed that as little as 0.1  $\mu\text{g}/\mu\text{L}$  Fe of folate nanoparticles captured viable A549 cells, reaching a plateau after 0.75  $\mu\text{g}/\mu\text{L}$  Fe (Figure 7A–E). In contrast, when we used the nonfunctionalized

nanoparticles, no cells were isolated (Figure 7F). Overall, these data indicate that our high-folate nanoparticle-based relaxation-mediated detection and subsequent magnetic isolation can be used in highly sensitive nondestructive assays.

Lastly, we utilized iron oxide nanoparticles' intrinsic peroxidase activity<sup>28,30,31</sup> for the colorimetric high-throughput confirmation of the expression of folate receptor (FR) on the membrane of magnetically captured and propagated A549 cells (Figure 8A). For these studies nonfluorescent folate iron oxide nanoparticles were used. After magnetically isolating and regrowing the A549 cells, 500 of these cells were incubated with increasing concentrations of high-folate nanoparticles. We found that the A549 cells in the presence of H<sub>2</sub>O<sub>2</sub> oxidized 3,3',5,5'-tetramethylbenzidine (TMB) (Figure 8B) in a nanoparticle-concentration-dependent fashion, indicating that the cells were viable and still expressing the FR. At nanoparticle concentrations above 1.2 Fe  $\mu\text{g}/\mu\text{L}$ , the absorbance reached a plateau. The control A549 cells, which were magnetically isolated with folate nanoparticles but incubated with nonfunctionalized nanoparticles, demonstrated nominal peroxidase activity. This indicates that the contribution of nanoparticles used for magnetic isolation is nominal toward the overall peroxidase activity. In contrast, the nonfolate-receptor-expressing H9c2 cells lacked any peroxidase activity (Figure 8B), as the folate nanoparticles did not associate with these cells. Through flow cytometry, we confirmed the expression of the FR in the

(30) Gao, L.; Zhuang, J.; Nie, L.; Zhang, J.; Zhang, Y.; Gu, N.; Wang, T.; Feng, J.; Yang, D.; Perrett, S.; Yan, X. *Nat. Nanotechnol.* **2007**, *2*, 577–583.

(31) Perez, J. M. *Nat. Nanotechnol.* **2007**, *2*, 535–536.

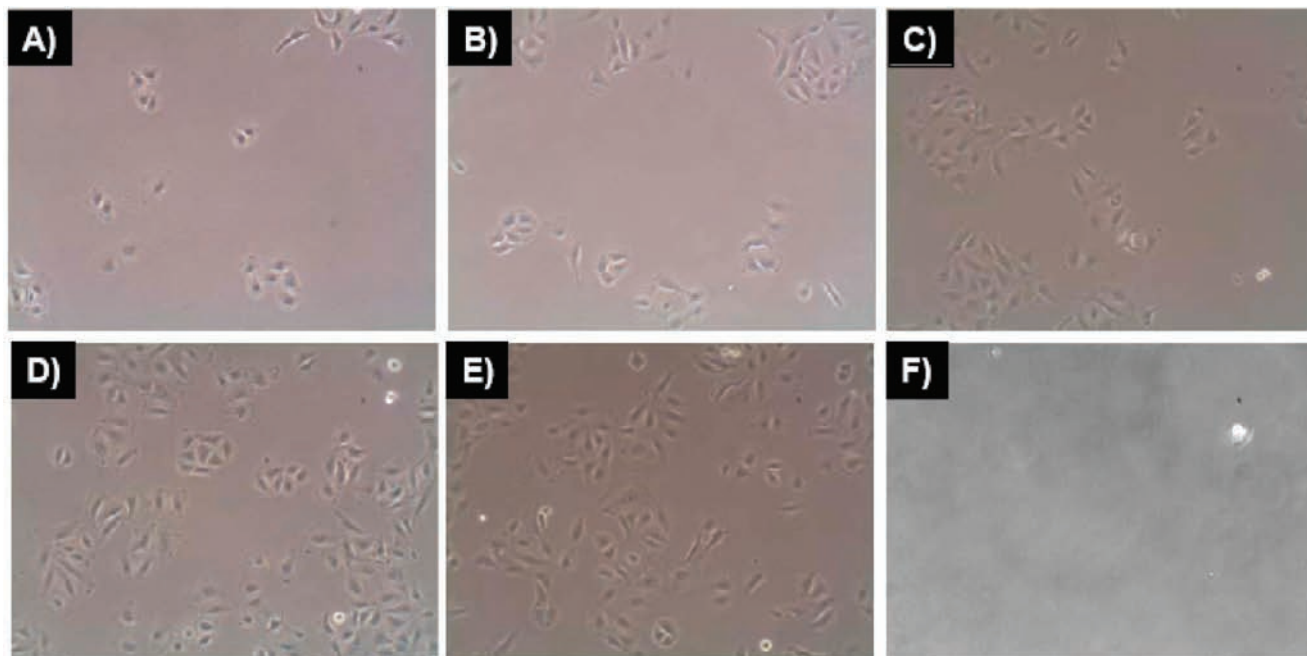


**Figure 7.** Folate nanoparticles facilitate the magnetic isolation of tumor cells expressing the folate receptor. The captured cells were grown at 37 °C, 5% CO<sub>2</sub> atmosphere, and visualized 24 h after isolation. Isolation of folate-receptor expressing cells with high-folate nanoparticles ((A) 0.1, (B) 0.25, (C) 0.5, (D) 0.75 and (E) 1 μg/μL Fe). (F) Absence of cell growth when nonfunctionalized nanoparticles were used (1 μg/μL Fe).

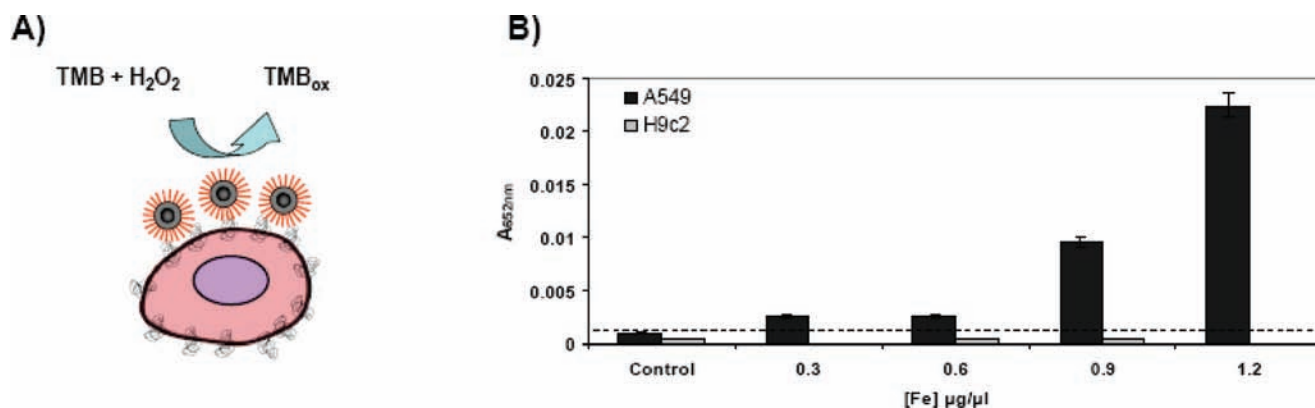


**Figure 8.** (A) Detection of cells using the folate nanoparticles' peroxidase activity. (B) Carcinoma cells (500 A549 cells) oxidize TMB, whereas rat cardiomyocytes (H9c2) do not. Cells were treated with nonfunctionalized nanoparticles (1.2 μg/μL Fe control) or different concentrations of high-folate nanoparticles (Means ± SE).

magnetically captured cells and its absence in the H9c2 control cells (SI Figure 7), thus corroborating the findings of nanoparticle-facilitated peroxidase assay (Figure 8B).

## Discussion

Nature widely employs highly selective multivalent interactions.<sup>1–11</sup> From enzymes and their substrates, to receptor–ligand pairs and antibody–antigen complexes, these associations are highly specific, despite being weaker than covalent interactions. For instance, the multivalent interaction between hemagglutinin of influenza virions and sialic acid moieties on bronchial epithelium cells mediates viral infection.<sup>7</sup> Specifically, recent studies indicate that multivalency, apart from participating in the initial attachment of a pathogen (i.e., virus, toxin) to a target cell, is critical for uptake via complex, highly regulated endocytic processes, in addition to direct fusion.<sup>32</sup> In line with

these observations, recently, a multivalent gold nanoparticle conjugate has been reported to transform a weakly binding and biologically inactive small molecule into a potent multivalent nanoagent that effectively inhibits HIV-1 fusion to human T cells.<sup>33</sup>

Considering the importance of multivalency on molecular recognition events, it is critical to assess its role in the sensitivity and detection pattern of novel nanoparticle-based diagnostic methods. Hence, in this report we addressed the fundamental question of how the nanoparticle valency affects the interaction of iron oxide nanoparticles with cells and what are the consequences in the magnetic-relaxation-mediated detection and magnetic isolation of these target entities. Our results indicate that nanoparticles with low valency switch from an assembled to a quasi-dispersed state as the target concentration increases,

(32) Miyauchi, K.; Kim, Y.; Latinovic, O.; Morozov, V.; Melikyan, G. B. *Cell* **2009**, *137*, 433–444.

(33) Bowman, M. C.; Ballard, T. E.; Ackerson, C. J.; Feldheim, D. L.; Margolis, D. M.; Melander, C. *J. Am. Chem. Soc.* **2008**, *130*, 6896–6897.



and this shift is accompanied with decrease in the  $\Delta T_2$ . On the other hand, nanoparticles with high valency move from a sparsely assembled to an extensive binding/clustering state, with a concomitant increase in  $\Delta T_2$  that is observed during this transition. Interestingly, similar results were obtained when mammalian or bacterial cells were used, suggesting that the previously reported differences in the detection of bacterial cells were attributed to the different levels of antibodies conjugated to the nanoparticles.<sup>17,28</sup> Additionally, the shift in the relaxation detection pattern is valency-regulated, as neither the matrix (blood vs milk), the ligand size (folate vs anti-FR), nor the nanoparticle's coating (herein polyacrylic acid vs dextran in previous reports<sup>17,28</sup>) affected the quantification trend. Hence, valency engineering should be a critical aspect in the synthesis of sensitive magnetic relaxation nanosensors and perhaps other nanoparticle-based diagnostic assays.

Another important element in the design of robust and affordable nanosensors is the utilization of nonlabile and readily available probes. In our studies, nanoparticles with high small molecule valency (high-folate nanoparticles) facilitated single cell detection and quantification in whole erythrocyte-containing blood, outperforming their low valency counterparts (low-folate nanoparticles) and antibody-carrying nanosensors (low- or high-anti-FR nanoparticles). Therefore, as it was recently demonstrated that even a single metastatic cancer progenitor cell can successfully induce tumor formation,<sup>29</sup> high-folate carrying nanoparticles may be used for the early detection of tumor cells in blood that overexpress the folate receptor. Furthermore, as the iron oxide nanoparticles can be easily conjugated via "click chemistry", other small molecules may be used for the synthesis of high-valency nanosensors, capable of detecting rare circulating tumor cell in blood that may express other biomarkers. Small molecules, apart from being cheaper and more robust than antibodies, can offer comparable specificity and can be easily utilized for the engineering of the nanoparticle valency, due to their minimal steric hindrance. Since small-molecule-carrying nanoparticles can sense single cells, as opposed to antibody-carrying nanoparticles, the wider utilization of small molecules in molecular diagnostics is expected. For instance, bacteria can

be targeted with small molecules screened from combinatorial libraries, leading to the development of bacterium-specific small-molecule-carrying nanoparticles, which can achieve reliable and sensitive detection at the points-of-care and in the developing world.

## Conclusion

We have demonstrated the role of iron oxide nanoparticle's ligand valency in (1) the rapid single cell detection of cancer cells in blood, (2) the magnetic isolation of cells for regrowth and further analyses, and (3) the corroboration of the presence of molecular targets in cultured cells' plasma membrane through a high-throughput cellular ELISA format. Finally, as we acknowledge the benefits of iron oxide nanoparticle-based assays and small molecule ligands, as well as the recent advancements in portable magnetic relaxation instrumentation,<sup>34</sup> we anticipate their broader use in the clinic and the field, expediting diagnosis and decision-making in cancer and infectious diseases.

**Acknowledgment.** We thank Dr. Saleh Naser (Burnett School of Biomedical Sciences, College of Medicine, UCF) for providing MAP and the anti-MAP antibody, Dr. James Hickman (Nanoscience Technology Center, UCF) for providing the fresh rat blood and the FITC-conjugated antibody, Mercedes Gonzales (Nanoscience Technology Center, UCF) for cell quantification, and Dr. Annette Khaled and Mounir Chehtane (Burnett School of Biomedical Sciences, College of Medicine, UCF) for their technical assistance in flow cytometry. This work was supported by the NIH grants CA101781 and GM084331 to J.M.P.

**Supporting Information Available:** (1) Nanoparticle characterization, (2) DLS of bacterial nanosensors, (3) correlation coefficients of time-dependent magnetic relaxation studies, and (4) determination of the expression of folate receptor via flow cytometry. This material is available free of charge via the Internet at <http://pubs.acs.org>.

JA9041077

(34) Lee, H.; Sun, E.; Ham, D.; Weissleder, R. *Nat Med* **2008**, *14*, 869–874.